IEEE Access
Multidisciplinary | Rapid Review | Open Access Journal

IEEE ON IEEE ENGINEERING IN MEDICINE AND BIOLOGY SOCIETY SECTION

Received February 22, 2020, accepted March 21, 2020, date of publication March 31, 2020, date of current version April 16, 2020.

Digital Object Identifier 10.1109/ACCESS.2020.2984677

The Abnormal Detection of Electroencephalogram With Three-Dimensional Deep Convolutional Neural Networks

DU YUN-MEI[1,2], ALLAM MAALLA[2], LIANG HUI-YING[1], HUANG SHUAI[1], LIU DONG[1], LU LONG[1,3,4], AND LIU HONGSHENG[1]

[1]Guangzhou Women and Children's Medical Center, Guangzhou Medical University, Guangzhou 510623, China
[2]School of Information Technology and Engineering, Guangzhou College of Commerce, Guangzhou 511363, China
[3]School of Information Management, Wuhan University, Wuhan 430072, China
[4]Division of Biomedical Informatics, Cincinnati Children's Hospital Medical Center, Cincinnati, OH 45229, USA

Corresponding author: Allam Maalla (allammaalla@yahoo.com)

This work was supported in part by the National Key Research and Development Project under Grant 2018yfc1315400, in part by the Guangdong Province's Colleges and Universities Innovation Project (Natural Science) under Grant 2018KTSCX262, and in part by the Guangdong Province Project, Construction of Teaching Team in Guangdong Province's Colleges and Universities Project under Grant 2019SJJXTD01.

ABSTRACT In this work, we present and evaluate a three dimensional Convolutional Neural Network algorithm to accurately detect EEG abnormalities from multi-channel EEG signals. This research synthesizes several heterogeneous datasets, constructs a dataset 10 times larger than other datasets of its kind, uses all channel EEG signals as input, and preprocesses them into data structures that can reflect EEG spatio-temporal character, constructs and trains a 28-layer deep residual network, automatically extracts high-level features, and recognizes EEG anomalies. We collect and reorganize several heterogeneous data sets, and convert two-dimensional signal segments to three-dimensional frames after preprocessing. Thus we build a dataset of 14049 annotated samples with shape 512*11*11*1, of which 8866 are abnormal. On this dataset, we train a 28-layer convolutional network with residual blocks which classify EEG segments as normal or abnormal. Prediction on independent test sets using this trained model achieved an accuracy of 96.67%. The AUC is 99.93% and the RMSE is 0.0032. We compared the results of several methods and found that 3D frame data structure and deeper CNN model is better. The performance of our model also outperforms other related researches on EEG classification.

INDEX TERMS Electroencephalogram (EEG), deep learning, 3D CNN, ResNet, EEG classification.

I. INTRODUCTION

Electroencephalogram (EEG) is the most efficient medical imaging tool to analyze and interpret the characteristics of the brain disorder which helps the physician to diagnose the level of consciousness, sleep disorders, epilepsy, tumors, lesions etc [1]–[2]. EEG is more and more widely used because of its unique advantages such as non-invasive, low cost, high time resolution and easy to use. At present, the role of EEG is greatly underestimated.

In clinical practice, brain wave abnormality detection from EEG recordings is usually performed by expert technicians and physicians given the high error rates of computerized interpretation [3]. Direct visual inspection is dull, time-consuming, inefficient, and lacks unified objective criteria, which can easily lead to misjudgments and omissions. The consistency among assessors (IRA) is also low. Automated examination is difficult because of the complexity of EEG signal itself, the polymorphism of abnormal discharge wave, the difference of fluctuation patterns among patients, and the presence of noise.

The research methods of EEG automatic detection are mainly divided into two categories.

1. Heuristic manual feature design and traditional machine learning methods. Conventionally, time or frequency domain features in EEG were extracted manually. Meanwhile, classifiers such as Support Vector Machine (SVM) and K-Nearest Neighbors (KNN)

The associate editor coordinating the review of this manuscript and approving it for publication was Michael Friebe.

were implemented. Researchers must devote numerous efforts to find and design various features from origin noisy signals. And the computation of these features is time consuming [4].

2. Deep learning is applied to automatic feature detection and hierarchical feature extraction. This method does not carry out manual feature extraction and selection, but uses the network to automatically learn features and then classify and recognize them. Many of these studies only use single channel EEG signal as input and discard other multi-channel signal information [5]. Some studies incorporate multi-channel signals, but only consider the time factor and drop the location information between channels [6]. Some take spatial factors into account, but adopt shallow network structure, which cannot fully extract higher-level features [7]–[8]. In addition, large amounts of data are essential for deep learning, which is the shortcoming of many studies that only use a single open data set.

II. DATA

A. SIGNAL DENOISING AND ARTIFACTS ELIMINATION

The EEG signal recorded on the scalp surface is very weak, usually only tens to hundreds of microvolts (μV). It is particularly susceptible to external and internal noise, such as muscle, eye, heart activity, line interference, electrode noise, electromagnetic interference in the environment, etc [14]–[15]. Therefore, before further analysis, the EEG signal is first de-noised and de-falsified. In this study, we use the wavelet transform and hierarchical threshold scheme to de-artifact and de-noise EEG. The original EEG signal is decomposed into 8 layers of wavelet coefficients by wavelet transform, each layer of coefficients is denoised by hierarchical threshold (HT), and then the denoised EEG signal is reconstructed by the threshold coefficient [16]–[17]. It lays a good foundation for further EEG feature learning, extraction, and classification.

B. DATA RECONSTUCTION

EEG signal is very weak, which needs millions of times amplification to display. The core of the EEG instrument is the amplifier. An amplifier constitutes a channel. Amplifiers can be connected by different lead modes. Reference leads reflect the absolute potential difference between a single recording point and the reference point, while bipolar leads record the potential difference between two points. The placement of electrodes is generally referred to as the 10-20 system recommended by the International Electroencephalographic Society or the 10% system recommended by the American Electroencephalographic Association [21], as shown in Fig. 1a and b respectively.

We have collected many heterogeneous annotated data sets [2]–[10]. They have different channels (22∼40), different sampling frequencies (250∼512), and have different lead modes (some are reference leads and others are bipolar leads).

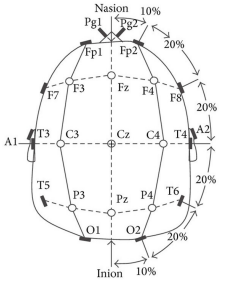

(a) International10-20 system

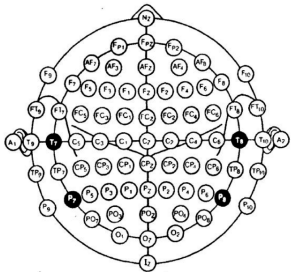

(b) American Electroencephalogram Association 10%system

FIGURE 1. Name and location of electrode.

TABLE 1. Name revisions referring to 10% system of the American EEG association.

Original Name	Amended Name	Original Name	Amended Name
EEGT3-REF	EEG T7-REF	EEG T6-REF	EEG P8-REF
EEG T4-REF	EEG T8-REF	EEG T1-REF	EEG FT9-REF
EEG T5-REF	EEG P7-REF	EEG T2-REF	EEGFT10-REF

Considering the distribution of data and the possibility of conversion, we unified the frequency to 256Hz and the channel to 22 bipolar leads (See Appendix 1 for sample bipolar lead data and Appendix 2 for reference leads with 32 channels as an example). Through interpolation or down sampling, all EEG data were sampled at a frequency of 256 Hz.

The method of reconstructing reference leads to bipolar leads is slightly complicated. Firstly, the channel name of the EEG signal is read from the source file, and the reference lead name is revised by referring to the 10% system of the American EEG Association. As shown in Table 1.

Secondly, the mapping relationship between the bipolar lead channel and the reference lead channel is determined. The formula is: Xj-Yj= EEG Xj-REF- EEG Yj-REF

The examples of mapping relationship are shown in Table 2.

This research intends to use a three-dimensional convolution neural network to process time-series data. The data are reconstructed and unified into 22*sampling points, and then divided into EEG segments with the growth of 2 seconds. In order to avoid over-fitting, we have made accurate segmentation without overlapping. With a 2-second time window and a 2-second sliding step, the EEG segment is captured by moving along the time direction. Because there are 256 sampling points per second, the structure of each EEG segment is like 22 * 512, and contains only one type of EEG

TABLE 2. Schedule 4 examples of electrode lead names and conversion relationships.

J	BipolarLlead Channel Mame **Xj—Yj**	Reference Lead Conversion Relations EEG **Xj**-REF—EEG **Yj**-REF
1	FP1—F7	EEG FP1-REF—EEG F7-REF
2	F7—T7	EEG FP2-REF—EEG T7-REF
3	T7—P7	EEG F3-REF—EEG P7-REF
4	P7—O1	EEG F4-REF—EEG O1-REF
5	FP1—F3	EEG FP1-REF—EEG F3-REF

signal (normal/abnormal). As for the length of time window, we have done experiments of one second, two seconds, five seconds, ten seconds and twenty seconds respectively. The experimental results show that two seconds is a better length of time window.

After shuffling the signal segments and their labels, the training set and test set are cut out. Thus we got a dataset of 14049 annotated samples, of which 8866 are abnormal. 2810 samples were selected as test sets and did not participate in model training.

C. DATA PREPROCESSING BASELINE SUBTRACTION

The individual differences in EEG signals are very large, especially in children and adults. We use the subtracting baseline procedure to eliminate individual differences. Firstly, the individual baseline is obtained by averaging the first N sampling points of each EEG record, and then all sampling points are subtracted from the baseline to obtain a new signal sequence.

EEG signals have a 2-D shape of channels*time, which lost the topological position information of the electrodes. Each channel has only one or two adjacent electrodes, while the physical electrodes have 4-8 adjacent electrodes. To include this information, according to the electrodeposition distribution of the 10-20 system, the channel sequence is reduced to the electrodeposition matrix sequence. The mapping relationship is shown in Figure 2.

The number in the lower right corner matrix is the number of the left channel, indicating the actual position of each channel. Each sampling point has 22 channels of potential data, mapped to an 11*11 matrix (frame) according to the position relationship so that the two-dimensional channel sequence can be converted into a three-dimensional frame sequence (512*11*11), as shown in Figure 3.

In this way, signals that come from physically adjacent channels are still adjacent in the frame, so the spatial information can be retained. The two-dimensional original data is transformed into three-dimensional training input, as shown in Figure 3.

D. MODEL ARCHITECTURE AND TRAINING

We use a 3-D convolutional neural network to learn the features of ECG and classify whether it is normal or not. CNN is well suited to identify simple patterns in data and then to form more complex patterns at higher levels. The 3D CNN is very effective when the feature of interest is obtained from the short (fixed length) fragments of the whole data set

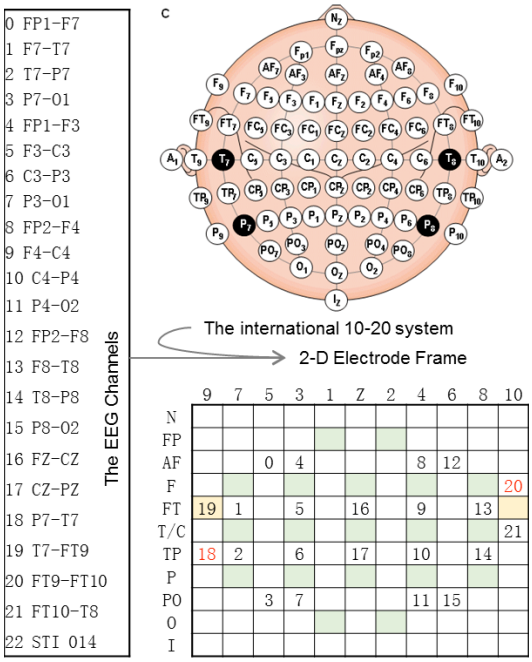

FIGURE 2. Mapping relationship between channel number and electrode position.

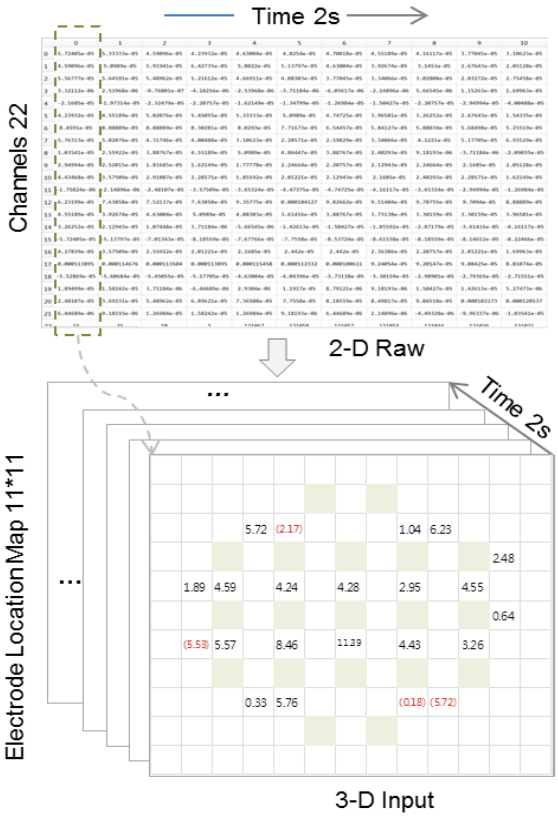

FIGURE 3. Converting a two-dimensional signal segment (22*512) to three-dimensional frames (512*11*11).

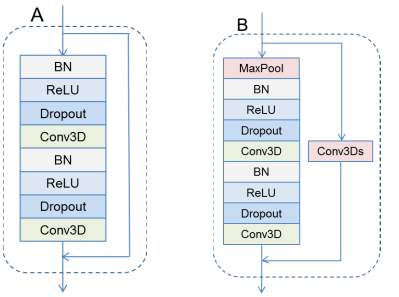

FIGURE 4. Residual block structure.

TABLE 3. The details of CNN strcture.

Module name	Kernel_size	Strides
Conv3D	[10,3,3]	[1,1,1]
Conv3Ds	[1,1,1]	[4,2,2]
MaxPool	pool_size=(4,2,2)	padding="same"
AvePool	pool_size=(4,2,2)	

* Module name: corresponding to the name of the boxes in Figure 4

and the location of the feature in the fragments are not highly correlated [18]–[20].

The high-level architecture of the network is shown in Figure 4. The network receives input (sample number, 512, 11, 11, 1) and outputs category prediction (sample number, 2) for each sample.

The depth of the deep learning network has a great influence on the final classification and recognition effect. To make the optimization of such a network tractable, we similarly employ shortcut connections to those found in the Residual Network architecture [3]–[19].

The network consists of two types of Residual block: one is identity block (A), each with two convolution layers, as shown in Figure 4 (a); and the other is a convolutional block (B). In the main path of this kind of block, the input is firstly pooled. The convolution operation with the same coefficients is carried out on the corresponding fast connection path to achieve the purpose of reducing sampling, as shown in Figure 4 (b).

Before each convolutional layer, we apply Batch Normalization, rectified linear activation and Dropout, adopting the pre-activation block design. The whole network consists of 9 identity blocks and 3 convolutional blocks. Its structure is shown in Figure 5. Among them "×3" means that the three residual blocks of "B-A-A" are stacked and repeated three times. The size of the filters in each layers are shown in Table 3. The number of filters in each convolution layer is shown on the right side of Figure 5 (numbers after @), started at 32, and doubled every four residual blocks. The last full connection layer is activated by SoftMax, giving the classification of each EEG time segment.

The network model is implemented by Keras in-depth learning framework. We train the networks from scratch, using x_train (11239, 512, 11, 11, 1), y_train(11239, 2), optimizer=Adam(0.001), loss="categorical_crossentropy", metrics=["accuracy",rmse]. After experimental comparison, Batch-size is set to 64 and Epoch is set to 50.

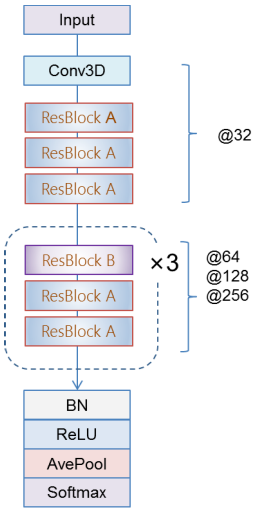

FIGURE 5. Model Architecture (3D-CNN 28).

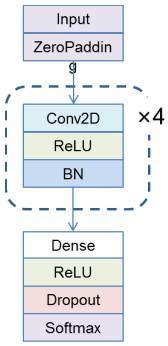

FIGURE 6. Model Architecture (2D-CNN 4).

III. EXPERIMENTS AND RESULTS

A. EXPERIMENTS

To verify the validity of the model, we have carried out several representative experiments asymptotically in terms of data volume, convolution type, and network depth. All experiments use the same training set and test set, and only slightly change the shape and format of the input data. Firstly, a shallow network structure consisting of only four convolution layers was constructed; network structure is shown in Figure 6.

Firstly, half of the training data were used to learn and classify (2D-CNN 4h), and the accuracy rate of the test set is 89.26%. Secondly, all the data were used to train (2D-CNN 4). The accuracy was improved by 2 percentage points. Then, using the same deep network structure mentioned above (Figure 4), but only doing two-dimensional convolution (2D-CNN 28), the accuracy is improved by nearly two percentage points, that is, the high-level features of time dimension are not excavated except for the first level. Finally, the three-dimensional deep model of this paper is used to train

TABLE 4. Expermintal design, loss and accuracy of each model on test set.

	2D-CNN 4h	2D-CNN 4	2D-CNN 28	3D-CNN 28
Training set size	5587	11239	11239	11239
Input shape	512,11,11	512, 11, 11	512, 11, 11	512, 11, 11, 1
Test set size	1397	2810	2810	2810
Test loss:	0.6657	0.4681	0.3920	0.1276
Test accuracy:	0.8926	0.9177	0.9241	0.9669

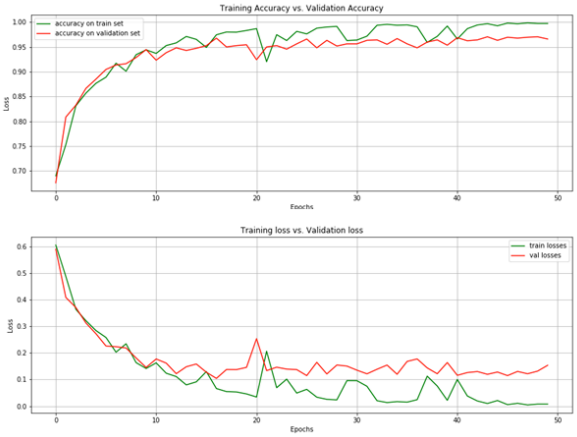

FIGURE 7. The accuracy and loss in training process.

(3D-CNN 28) and mine the spatial and temporal characteristics at the same time.

We split the dataset into a training and validation set. The training set contains 90% of the data. The parameters, accuracy and loss rates of several models are shown in Table 4.

It can be seen that the amount of data has a greater impact on the training effect, using as much data as possible to train the network; besides, the effect of deep network is better than that of shallow model; moreover, three-dimensional convolution is more effective than two-dimensional convolution, which further improves the accuracy. In our other project, we also try to use one-dimensional convolution depth network to detect EEG abnormalities [22], and the results show that the effect of three-dimensional convolution is still better.

B. TRAINING

The model of this research (3D-CNN 28) is training on a server equipped with 24G Nvidia M6000 GPU. It takes about 18 hours to train 50 epochs.

We uses the following evaluation indicators to visually show the performance of the model training process. The accuracy and loss of the training set and the verification set are shown in Figure 7 respectively.

Two other indicators RMSE and AUC are also defined in the training process. We use root mean square error (RMSE) to measures the deviation between the predicted value and the true value, as shown in Formula 1.

$$rmse(y\_true, y\_pred) = \sqrt{\frac{1}{n}\sum_{i=1}^{n}(y\_pred - y\_true)^2} \quad (1)$$

AUC value is the area covered by the ROC curve. The bigger the AUC value is, the better the classification effect is.

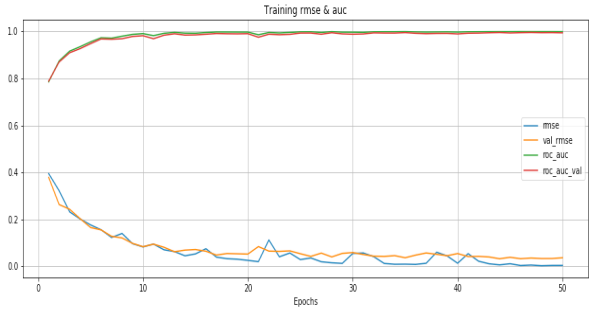

FIGURE 8. The RMSE and AUCin training process.

TABLE 5. Obfuscation matrix ontest set.

0.96 (1027)	0.04 (48)
0.02 (37)	0.98 (1698)

TABLE 6. Model performance on test set.

	Precision	Recall	F1-score	Support
0	0.97	0.96	0.96	1075
1	0.97	0.98	0.98	1735

The callback function is used here, and each epoch is calculated once. The change process of AUC and RMSE is shown in Figure 7, the below two curves are RMSE and average RMSE, and the above two curves are AUC and average AUC. The accuracy rate of the last epochs is 99.86, the AUC is 99.93 and the variance is reduced to 0.0032.

C. RESULTS

Test sets are independent data that do not participate in model training. The trained model is used to predict on the test set, and the tabulated confusion matrix is presented in Table 5. It can be seen that 98% of abnormal EEG signals are correctly classified as abnormal, and 96% of normal EEG signals are correctly classified as normal. The performance of the proposed model is summarized in Table 6.

IV. ANALYSIS

EEG signal is weak and vulnerable to interference. In this study, we firstly use a hierarchical threshold scheme to de-artifact EEG signals and try to eliminate the interference of other non-EEG signals.

The individual differences in EEG signals are quite large, especially in children and adults. We use the subtracting baseline procedure to eliminate individual differences. The data set used in this study contains both children's and adults' EEGs, but we do not distinguish age groups. The results show that the baseline subtraction (2D-CNN 4h and 2D-CNN 4 in Table 3) achieves the purpose of eliminating individual differences. The original data with great differences are combined with training models to achieve better classification accuracy.

Besides, the reconstruction and pre-processing of multiple heterogeneous data sources not only increases the amount of training and testing data but also improves the training and

TABLE 7. Comparison between our work and other related research.

Model	Accuracy
5-layer 3D CNN [8]	73.1%
5-layer 1D CNN [12]	81.6%
13-layer deep 1D CNN [5]	88.7%
8-layer 3D CNN+2LSTM [7]	88.9%
3-layer 2D CNN+LSTM [13]	91.0%
28-layer 3D CNN [our]	97.9%

classification effect, as well as the generalization ability and robustness of the model.

Two-dimensional EEG data structure loses the position information of electrodes. We transform the two-dimensional channel sequence (512*22) into a three-dimensional frame sequence (512*11*11) by restoring mapping. Then we use 3D-CNN to capture the temporal and spatial dynamic changes of EEG signals simultaneously. The experimental results show that the three-dimensional convolution is more effective than two-dimensional and one-dimensional convolution (2D-CNN 28, 3D-CNN 28 in Table 4).

The depth of the neural network has a great influence on the performance of the model, such as 2D-CNN 4 and 3D-CNN 28 in Table 4. The effect of the deep network is better than that of the shallow model. We also compared other similar studies using three-dimensional convolution neural network to classify EEG (such as 5-layer 3D CNN [8] 73.1%, 8-layer 3D CNN + 2LSTM [7] 88.9%, 28-layer 3D CNN [our] 97.9%). The model depth and the final classification accuracy are shown in Table 7. It can be seen that the recognition and detection of EEG using a deeper CNN is the right direction. It is also the consensus of the research community to make the neural network deeper, because the deeper the layers are, the more high-level features can be learned. In this paper, the ResNet residual unit is introduced to solve the problem of deep network degradation and vanishing gradient.

We also compare our model with five different related approaches. Although these models are based on different data sets and have different research fields, they all attempt to use CNN for EEG classification and recognition. Table 7 summarizes the classification accuracy of these studies. Table 6 demonstrates that the 28-layer 3D CNN method outperforms the others and improves the average accuracy by nearly 7-15%.

V. CONCLUSION

In this paper, we develop a model to automatically extract Spatio-temporal features and classify EEG segments as normal or abnormal from multi-channel signals. Main points to the performance of the model are 3D frame data structure, a very deep convolutional network with residual blocks, three-dimensional conversion of EEG Signals and a relatively large integrated data sets. We achieved a high average accuracy at 88.7%, AUC at 0.9993, and a low RMSE at 0.0032.

Further work includes clinical verification, research on the interpretability of deep learning model, and explore the basis of the model to give the diagnosis results.

APPENDIX

Appendix 1. The data example: 22 channel bipolar lead.

	Name \ Time	t1	t2	t3	t4
0	FP1-F7	1.63E-04	1.95E-07	5.86E-07	3.32E-06
1	F7-T7	-1.86E-04	1.95E-07	-1.95E-07	-2.93E-06
2	T7-P7	-2.15E-06	1.95E-07	1.95E-07	5.86E-07
3	P7-O1	2.48E-05	1.95E-07	1.95E-07	9.77E-07
4	FP1-F3	9.57E-06	1.95E-07	1.95E-07	5.86E-07
5	F3-C3	-8.40E-06	1.95E-07	1.95E-07	9.77E-07
6	C3-P3	3.32E-06	1.95E-07	1.95E-07	1.95E-07
7	P3-O1	-4.49E-06	1.95E-07	1.95E-07	-1.95E-07
8	FP2-F4	-1.93E-05	1.95E-07	1.95E-07	1.95E-07
9	F4-C4	-1.47E-05	1.95E-07	1.95E-07	1.95E-07
10	C4-P4	6.06E-06	1.95E-07	1.95E-07	1.95E-07
11	P4-O2	-1.93E-05	1.95E-07	1.95E-07	1.95E-07
12	FP2-F8	8.22E-05	1.95E-07	5.86E-07	2.93E-06
13	F8-T8	-8.58E-05	1.95E-07	-1.95E-07	-2.15E-06
14	T8-P8-0	-1.78E-05	1.95E-07	1.95E-07	1.95E-07
15	P8-O2	-2.60E-05	1.95E-07	1.95E-07	1.95E-07
16	FZ-CZ	-3.18E-05	1.95E-07	1.95E-07	1.95E-07
17	CZ-PZ	5.27E-06	1.95E-07	1.95E-07	5.86E-07
18	P7-T7	2.54E-06	1.95E-07	1.95E-07	-1.95E-07
19	T7-FT9	8.40E-06	1.95E-07	1.95E-07	1.95E-07
20	FT9-FT10	4.24E-05	1.95E-07	1.95E-07	1.95E-07
21	FT10-T8	-8.79E-06	1.95E-07	1.95E-07	1.95E-07

Appendix 2. The data example: 32 channel reference lead.

	Name \ Time	t1	t2	t3	t4
0	EEG FP1-REF	-3.60E-05	-3.60E-05	-3.60E-05	-3.78E-05
1	EEG FP2-REF	-2.52E-05	-2.52E-05	-2.43E-05	-2.43E-05
2	EEG F3-REF	-2.61E-05	-2.52E-05	-2.52E-05	-2.70E-05
3	EEG F4-REF	-7.19E-06	-6.29E-06	-6.29E-06	-7.19E-06
4	EEG C3-REF	-8.09E-06	-8.09E-06	-8.09E-06	-8.99E-06
5	EEG C4-REF	6.31E-06	7.21E-06	6.31E-06	5.41E-06
6	EEG P3-REF	6.31E-06	7.21E-06	4.51E-06	4.51E-06
7	EEG P4-REF	1.44E-05	1.44E-05	1.26E-05	1.26E-05
8	EEG O1-REF	1.53E-05	1.53E-05	1.53E-05	1.35E-05
9	EEG O2-REF	2.07E-05	1.89E-05	1.89E-05	1.71E-05
10	EEG F7-REF	-3.78E-05	-3.69E-05	-3.69E-05	-3.60E-05
11	EEG F8-REF	-8.99E-06	-8.09E-06	-8.99E-06	-9.89E-06
12	EEG T3-REF	-2.34E-05	-2.34E-05	-2.34E-05	-2.52E-05
13	EEG T4-REF	3.61E-06	2.71E-06	3.61E-06	2.71E-06
14	EEG T5-REF	1.00E-08	-1.79E-06	-1.79E-06	-2.69E-06
15	EEG T6-REF	1.62E-05	1.53E-05	1.53E-05	1.35E-05
16	EEG FZ-REF	-1.98E-05	-1.89E-05	-1.80E-05	-2.07E-05
17	EEG CZ-REF	6.31E-06	4.51E-06	4.51E-06	2.71E-06
18	EEG PZ-REF	1.44E-05	1.53E-05	1.44E-05	1.26E-05
19	EEG EKG-REF	4.51E-06	1.00E-08	4.51E-06	7.21E-06
20	EEG A1-REF	7.21E-06	-9.89E-06	-2.16E-05	-1.89E-05
21	EEG A2-REF	4.51E-06	9.10E-07	-3.59E-06	-8.90E-07
22	EEG T1-REF	-3.15E-05	-3.06E-05	-3.06E-05	-3.24E-05
23	EEG T2-REF	-8.90E-07	-1.79E-06	-8.90E-07	-1.79E-06
24	EEG SP1-REF	1.17E-05	-9.89E-06	-2.25E-05	-2.07E-05
25	EEG SP2-REF	1.00E-08	-7.19E-06	-6.29E-06	-8.09E-06
26	EEG LUC-REF	1.44E-05	-8.09E-06	-2.25E-05	-1.89E-05
27	EEG RLC-REF	-1.26E-05	-1.35E-05	-1.26E-05	-1.53E-05
28	EEG RESP1-REF	9.91E-06	-9.89E-06	-2.25E-05	-1.53E-05
29	EEG RESP2-REF	3.61E-06	-1.71E-05	-1.80E-05	-1.08E-05
30	EEG 31-REF	-8.99E-06	-8.09E-06	-8.99E-06	-8.99E-06
31	EEG 32-REF	-4.05E-05	-3.87E-05	-3.96E-05	-4.05E-05

ACKNOWLEDGMENT

(Du Yun-Mei and Allam Maalla are co-first authors.)

REFERENCES

[1] J. W. C. Medithe and U. R. Nelakuditi, "Study of normal and abnormal EEG," in *Proc. 3rd Int. Conf. Adv. Comput. Commun. Syst. (ICACCS)*, Coimbatore, India, Jan. 2016, pp. 1–4.

[2] A. Shoeb and J. Guttag, "Application of machine learning to epileptic seizure detection," in *Proc. 27th Int. Conf. Mach. Learn.*, Haifa, Israel, 2010, pp. 975–982.

[3] P. Rajpurkar, A. Y. Hannun, M. Haghpanahi, C. Bourn, and A. Y. Ng, "Cardiologist-level arrhythmia detection with convolutional neural networks," 2017, *arXiv:1707.01836*. [Online]. Available: http://arxiv.org/abs/1707.01836

[4] U. R. Acharya, Y. Hagiwara, and H. Adeli, "Automated seizure prediction," *Epilepsy Behav.*, vol. 88, pp. 251–261, Nov. 2018.
[5] U. R. Acharya, S. L. Oh, Y. Hagiwara, J. H. Tan, and H. Adeli, "Deep convolutional neural network for the automated detection and diagnosis of seizure using EEG signals," *Comput. Biol. Med.*, vol. 100, pp. 270–278, Sep. 2018.
[6] J. B. Yang, M. N. Nguyen, P. P. San, X. L. Li, and S. Krishnaswamy, "Deep convolutional neural networks on multichannel time series for human activity recognition," in *Proc. 24th Int. Joint Conf. Artif. Intell. (IJCAI)*, 2015, pp. 3995–4001.
[7] P. Zhang, X. Wang, W. Zhang, and J. Chen, "Learning spatial–spectral–temporal EEG features with recurrent 3D convolutional neural networks for cross-task mental workload assessment," *IEEE Trans. Neural Syst. Rehabil. Eng.*, vol. 27, no. 1, pp. 31–42, Jan. 2019.
[8] Y. Wang, Z. Huang, B. McCane, and P. Neo, "EmotioNet: A 3-D convolutional neural network for EEG-based emotion recognition," in *Proc. Int. Joint Conf. Neural Netw. (IJCNN)*, Rio de Janeiro, Brazil, Jul. 2018, pp. 1–7.
[9] (Jun. 9, 2010). *CHB-MIT Scalp EEG Database, Version: 1.0.0*. [Online]. Available: https://www.physionet.org/physiobank/database/chbmit/
[10] *Temple University Hospital EEG (TUH EEG) Resources*. [Online]. Available: https://www.isip.piconepress.com/projects/tuh_eeg/
[11] *Electroencephalography*. Accessed: Jan. 1995. [Online]. Available: http://www.bem.fi/book/13/13.htm#03
[12] K. G. van Leeuwen, H. Sun, M. Tabaeizadeh, A. F. Struck, M. J. A. M. van Putten, and M. B. Westover, "Detecting abnormal electroencephalograms using deep convolutional networks," *Clin. Neurophysiol.*, vol. 130, no. 1, pp. 77–84, Jan. 2019.
[13] Y. Yang, Q. Wu, M. Qiu, Y. Wang, and X. Chen, "Emotion recognition from multi-channel EEG through parallel convolutional recurrent neural network," in *Proc. Int. Joint Conf. Neural Netw. (IJCNN)*, Rio de Janeiro, Brazil, Jul. 2018, pp. 1–7.
[14] D. Yun-Mei, L. Hui-Ying, and H. Shuai, "Stream de-noising of children's EEG signals based on hierarchical thresholds," *China Digit. Med.*, vol. 3, no. 3, pp. 88–91, 2019.
[15] A. Maalla, C. Zhou, and G.-Y. Wu, "The construction of heterogeneous platform of unified service system based on cloud computing," in *Proc. CMEE*, Mar. 2018, pp. 678–682, doi: 10.12783/dtcse/cmee2017/20056.
[16] D. Yun-mei, L. Hui-ying, and H. Shuai, "Proprocessing of stream denoising for children's EEG signals based on hierarchical thresholds," *China Digit. Medicing*, vol. 14, no. 3, pp. 88–91, 2019, doi: 10.3969/j.issn.1673-7571.2019.02.025.
[17] A. Maalla, "Research on DC transmission operation system based on analyze the principle of Udi0," in *Proc. IEEE 4th Adv. Inf. Technol., Electron. Autom. Control Conf. (IAEAC)*, Chengdu, China, Dec. 2019, pp. 2580–2583.
[18] V. Indelman, S. Williams, M. Kaess, and F. Dellaert, "Information fusion in navigation systems via factor graph based incremental smoothing," *Robot. Auto. Syst.*, vol. 61, no. 8, pp. 721–738, Aug. 2013.
[19] A. Maalla, "Construction of information ecosystem on enterprise information portal (EIP)," *J. Electr. Electron. Syst.*, vol. 5, p. 205, Jan. 2016, doi: 10.4172/2332-0796.1000205.
[20] J. Malmivuo and R. Plonsey, *Bioelectromagnetism*. New York, NY, USA: Oxford Univ. Press, 1995. [Online]. Available: http://www.bem.fi/book/13/13.htm#03
[21] A. K. Farhan, R. S. Ali, H. Natiq, and N. M. G. Al-Saidi, "A new S-box generation algorithm based on multistability behavior of a plasma perturbation model," *IEEE Access*, vol. 7, pp. 124914–124924, 2019.
[22] Y.-M. Du, H.-Y. Liang, and S. Huang, "The detection of anomaly in electroencephalogram with deep convolutional neural networks," *J. South China Normal Univ., Natural Sci. Ed.*. vol. 52, no. 2, pp. 122–128, 2020, doi: 10.6054/j.jscnun.2020035.

DU YUN-MEI received the B.S. degree in computer science from the Kunming University of Science and Technology. She is currently a Data Analyst with the Guangzhou Women and Children's Medical Center and an Associate Professor with the Guangzhou College of Commerce. Her main research directions are artificial intelligence and intelligent application of medical big data.

ALLAM MAALLA received the master's degree in communication and information engineering and the Ph.D. degree in communication and information engineering from the Wuhan University of Technology, China, in 2007 and 2010, respectively. He is currently a Professor with the School of Information Technology and Engineering, Guangzhou College of Commerce. His research interests include big data analysis, data-intensive computing, cloud computing, and virtualization technology.

LIANG HUI-YING received the Ph.D. degree from Southern Medical University. He is currently the Director of the Data Center of Guangzhou Women and Children's Medical Center. His main research direction is intelligent application of health care big data.

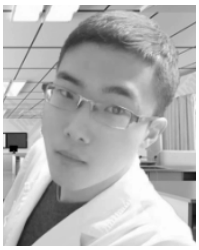

HUANG SHUAI graduated from the University of Science and Technology of China. He is currently working with the Data Center Department, Guangzhou Women and Children's Medical Center. His research interest involves the research of physiological signals, including ECG and EEG and related diseases.

LIU DONG graduated from the Guangzhou College of Commerce, in 2019. Since January 2019, he has been working with the Data Center Department, Guangzhou Women and Children's Medical Center. His research interests involve the research of network architectural search and computer vision.

LU LONG received the B.S. degree in biotechnology from Peking University, China, and the Ph.D. degree in computational biology from the School of Medicine, Washington University in St. Louis. He did Postdoctoral Training at Yale University. He is currently a Professor and the Ph.D. Supervisor with the School of Information Management, Wuhan University. His research interests include biomedical informatics and big data analysis and application.

LIU HONGSHENG received the Ph.D. degree in medicine. He is currently the Chief Physician and the Director of the Radiology Department, Guangzhou Women and Children Medical Center. It is mainly devoted to the comprehensive clinical application of MRI for women and children.